Invited Paper: 2003 Photonics West, Jan 29-Feb 03, 2003 Paper OE15-29-02

Design and Development of Short and Long Wavelength Infrared Vertical Cavity Surface Emitting Lasers

Agis A. Iliadis and A. Christou*

Electrical and Computer Engineering Department
University of Maryland, College Park MD 20742

*Department of Materials Science and Engineering and
Materials Research Science and Engineering Center,
University of Maryland, College Park MD 20742

ABSTRACT

The design, fabrication and performance of low threshold selectively oxidized infrared vertical cavity surface emitting lasers (VCSELs) for operation at 0.89μm and 1.55μm wavelengths using optimized graded Bragg mirrors, is reported. The devices are based on III-V ternary (AlGaAs/GaAs) and quaternary (AlInGaAs/GaInAsP/InP) graded semiconductor alloys and quantum wells and are grown by Molecular Beam Epitaxy. The VCSEL arrays are processed using inductively coupled plasma (ICP) etching with BCl_3 gas mixtures to achieve vertical walls and small geometries, and the fabrication of the devices proceeds by using conventional Ohmic contacts (Ti-Pt-Au and Ni-Au-Ge-Ni) and indium tin oxide (ITO) transparent contacts. The theoretical investigation of the optical properties of the quaternary compound semiconductor alloys allows us to select the optimum materials for highly reflective Bragg mirrors with less periods. The simulation of the designed VCSEL performance has been carried out by evaluation of the important laser characteristics such as threshold gain, threshold current density and external quantum efficiency.

1. INTRODUCTION

Compound semiconductor based IR surface emitting lasers are important light sources for large capacity optical communications and optical interconnection systems [1]. These devices exhibit in general such advantages as low threshold currents, single mode operation, high coupling efficiencies into optical fiber [2], and high speed modulation [3]. Development has focused on the investigation of structures and materials for highly reflective Bragg mirrors [4] and improved Ohmic electrodes. Transparent electrodes such as indium tin oxide (ITO) have been reported [5], but the best choice for high quality epitaxial mirrors has not yet been determined. The most commonly used material systems for the Distibuted Bragg Reflectors (DBRs) are AlGaAs/GaAs layers for the GaAs short-wavelength systems, or GaInAsP/InP for the longer wavelength systems, which requires the growth of 50 layer pairs to achieve a reflectivity of 99.9% [5,6,7], and AlGaInAs/AlInAs which requires the growth of 41 pairs for R=99.9% [8], thus showing the need for very thick structures to obtain high reflectivity Bragg mirrors. Higher refractive index contrast DBRs reported with fewer mirror pairs are based on the AlGaAsSb/AlAsSb material system [9,10]. These Bragg mirrors use only 20 pairs of alternating AlGaAsSb/AlAsSb layers to obtain reflectivity of 99%. However, these structures are easily degraded and are usually difficult to grow [11,12]. In this work, we report and review the design, fabrication and performance of a VCSEL structures for operation at short (0.89μm) and long (1.55μm) wavelength emission, based on the GaAs and InP systems respectively, with optimized DBRs and unstrained MQW active layers.

2. SHORT-WAVELENGTH VCSEL DESIGN AND DEVELOPMENT

The short-wavelength VCSEL structures consisted of a (12nm)$Al_{0.2}Ga_{0.8}As$/(10nm)GaAs (4x) QW active region, two 56.7nm $Al_xGa_{1-x}As$ (graded from x=0 to x=0.98) lateral oxidation layers, and two Bragg mirrors (DBRs), as shown schematically in Figure 1. The two Bragg mirrors consisted of graded $Al_{0.92}Ga_{0.08}As/Al_{0.12}Ga_{0.88}As$ alternating layers with each pair having a thickness of 130.68nm. The top DBR is p-type doped at concentrations of $2x10^{18}cm^{-3}$, and has 19 pairs

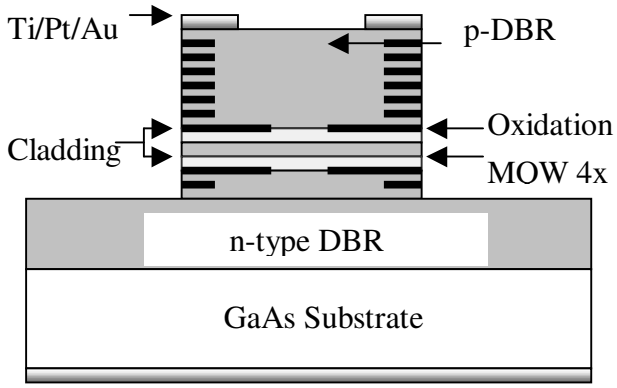

Figure 1. Schematic of 0.89µm VCSEL structure.

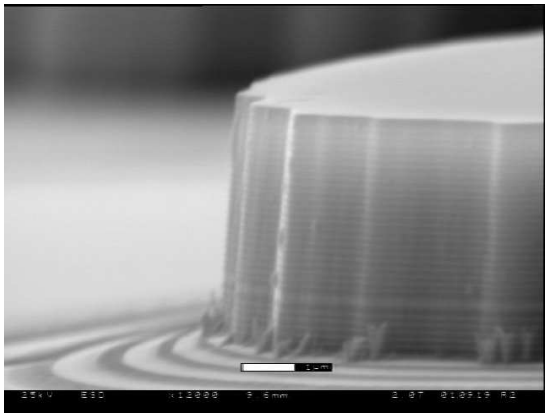

Figure 2. SEM micrograph of VCSEL.

for expected reflectivities of 97%, while the bottom DBR has 39 pairs for reflectivities of 99.9%,and it is doped n-type at concentrations of $2x10^{18}cm^{-3}$. This graded index separate confinement heterostructure (GRINSCH) is grown by MBE, and for the formation of the VCSEL arrays, standard photolithography is used for mesa and Ohmic contact formation. For mesa formation the structures were etched using inductively coupled plasma (ICP) dry etching in BCl_3/Cl_2 gas (12.5/2.5sscm). Under these conditions the etch rate was determined to be 323nm/min, and arrays of VCSELS were produced with vertical mesa walls as shown in Figure 2. P-type Ohmic contacts were deposited by e-beam evaporation and consisted of (10nm)Ti/(30nm)Pt/(250nm)Au, while the n-type contacts consisted of (5nm)Ni/(80nm)Au/(40nm)Ge/(30nm)Ni/(200nm)Au, and were annealed at 300 and 400 °C respectively. Figures 3 (a) and (b) show theoretically designed DBRs of a similar VCSEL structure emitting at 0.86µm containing two DBRs of 23 and 35 pairs with reflectivities of 97.8% and 99.8% respectively. Figure 4 shows the stimulated emission spectrum of the VCSEL lasing at 0.89µm.

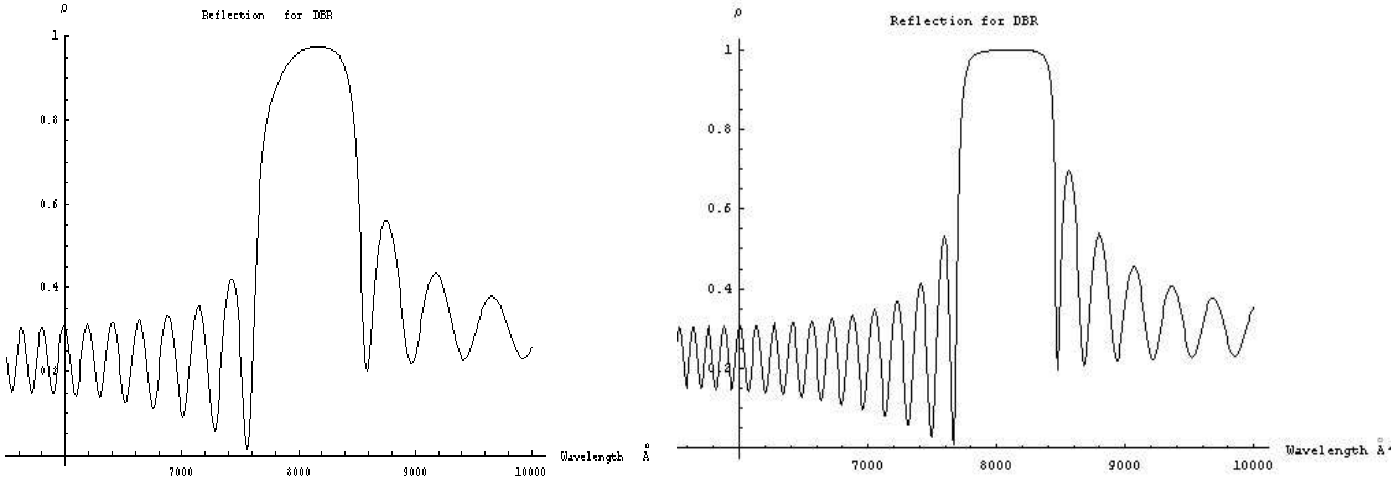

Figure 3(a). P-type DBR with 23 pairs and reflectivity 97.8%. (b). N-type DBR with 35 pairs and reflectivity 99.8%.

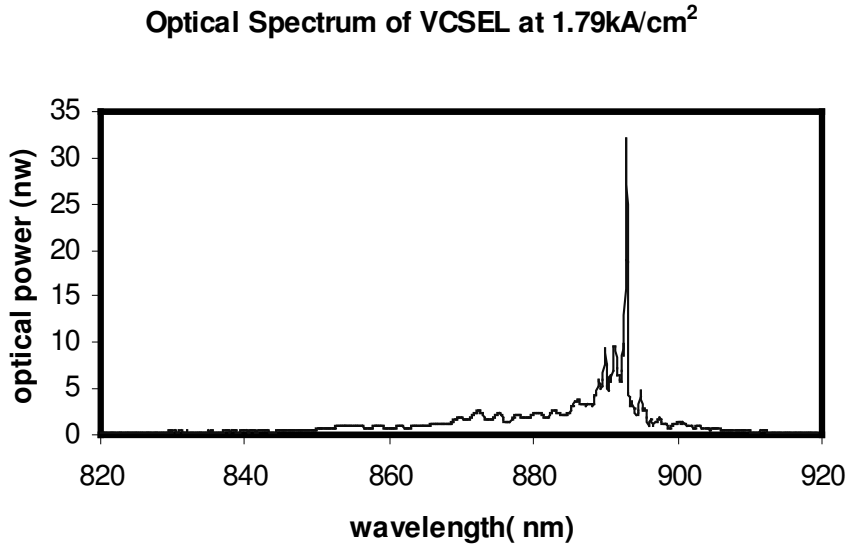

Figure 4. VCSEL stimulated emission spectrum lasing at 0.893μm.

3. LONG-WAVELENGTH VCSEL DESIGN AND DEVELOPMENT

Quaternary III-V semi-conductor alloys offer a high degree of flexibility in variation of their electro-optical properties, and play an important part in the development of new optical devices. In order to predict the dielectric constant behavior of the quaternary alloy, we initially consider the energy band gap dependence on the composition of quaternary semiconductor alloys. These results are then used for the calculation of the dielectric constant, which in turn allows us to select the alloys leading to the largest index of refraction contrast ratio.

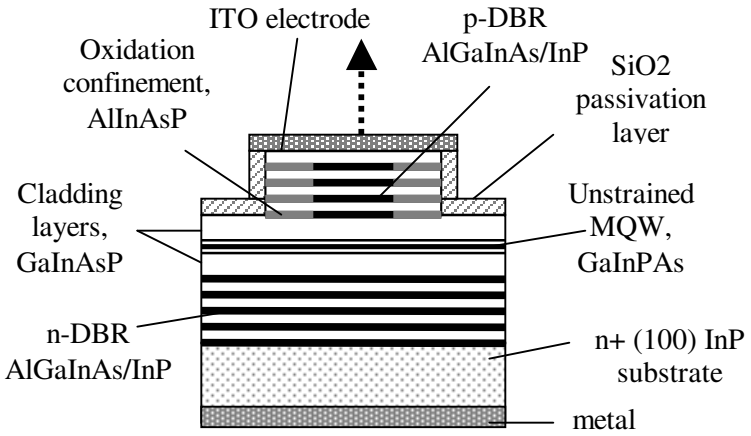

Figure 5. Schematic of long-wavelength VCSEL structure.

The estimation of the composition dependence of the quaternary semiconductor alloy energy gap has been demonstrated by Moon et al. [14], and is based on the material parameters of the four corresponding binary constituents. These parameters include values of the direct and indirect energy band gaps of the binary compounds as well as the bowing parameters of the ternary compounds. The method used for the calculation of the real and imaginary parts of the dielectric constant has been reported by Adachi [13]. It is based on a simplified model of the band structure of the materials [19] and covers the optical response of the semiconductors over the entire range of the photon energies. By calculating the imaginary part of the dielectric constant, ε_2, using the Kramers-Kronig relationships, and assuming parabolic behavior of the energy band gap of the semiconductor, the real part of the dielectric constant, ε_1, is obtained. As a result of this investigation, two material systems have been selected that are lattice matched to InP substrate and demonstrate the largest contrast between their refractive indices. $Al_{0.05}Ga_{0.42}In_{0.53}As$ and InP alloys have refractive indices of 3.8 and 3.17, respectively, resulting in refractive index difference of 0.63. Figure 5 presents the 1.55μm VCSEL structure, which is similar with the short-wavelength VCSEL shown in Fig. 1. The VCSEL is fabricated on n-type (001) InP substrate and includes two DBRs, cladding layers, unstrained MQW active layer and oxidizing layer where all materials are lattice matched to the substrate. The MQW structure in this VCSEL is unstrained and unintentionally doped. The MQW active region lasing at 1.546μm was theoretically designed and optimized, consisting of eight $Ga_{0.43}In_{0.57}As_{0.92}P_{0.08}$ wells, 6nm thick, separated by seven

$Ga_{0.23}In_{0.77}As_{0.5}P_{0.5}$ barriers, 9nm thick. The band gaps of the well (E_g = 0.78eV) and barrier (E_g = 1.0eV) layers were optimized to obtain the largest conduction band discontinuity for a sufficient quantum size effect of electrons [16]. The MQW layer was located at the peak of the electric field standing wave in order to achieve matched gain. The active region is spaced by the cladding layers: $Ga_{0.11}In_{0.89}As_{0.24}P_{0.76}$ and $Ga_{0.03}In_{0.97}As_{0.07}P_{0.93}$, with energy band gaps 1.2eV and 1.31eV, respectively. The thickness of $Ga_{0.11}In_{0.89}As_{0.24}P_{0.76}$ top cladding layer is 20nm, and $Ga_{0.03}In_{0.97}As_{0.07}P_{0.93}$ second top cladding layer is 81.6nm thick. $Ga_{0.11}In_{0.89}As_{0.24}P_{0.76}$ bottom cladding layer is 70nm thick and $Ga_{0.03}In_{0.97}As_{0.07}P_{0.93}$ bottom cladding layer is 101.1nm thick.

A single $Al_{0.22}In_{0.78}As_{0.47}P_{0.53}$ layer, 70nm thick, is introduced as the lowest layer in the p-type DBR next to the cladding layers to be used for selective oxidation in order to improve VCSEL efficiency through selective oxidation formation of an aperture [17]. The insulating buried oxide efficiently confines the charge carriers into the laser active region while the reduced refractive index of the oxide transversely confines the laser emission. In addition, the larger Al mole fraction of this layer results in selectivity for oxidation in comparison with the AlGaInAs of the Bragg layers. The oxidation of $Al_{0.22}In_{0.78}As_{0.47}P_{0.53}$ layer has been performed in a normal oven with water vapor produced adjacent to the oven at 85 C. The aperture diameter is controlled through the calibration of temperature and oxidation time with aperture diameter. The produced VCSEL core diameter was maintained at 7μm, using a mesa of 20-21μm.

The two Bragg mirrors of the VCSEL structure consist of $Al_{0.05}Ga_{0.42}In_{0.53}As$/InP alternating layers with refractive index difference of 0.63. The energy bandgaps of $Al_{0.05}Ga_{0.42}In_{0.53}As$ and InP have been found to be 0.8eV and 1.35eV, and their indices of refraction are 3.8 and 3.17, respectively. The top p-DBR is designed to be doped with Be at concentrations of about $10^{19}cm^{-3}$, and the bottom n-DBR is doped with Si up to 5 $x10^{18}cm^{-3}$. The quarter wavelength thicknesses of $Al_{0.05}Ga_{0.42}In_{0.53}As$ and InP alternating layers for both DBRs have been calculated to be 101.7nm and 121.9nm, respectively. The expected mirror reflectivities are 97% for the top DBR consisting of 16 pairs of $Al_{0.05}Ga_{0.42}In_{0.53}As$/InP layers, and 99.9% for the bottom DBR consisting of 22 pairs.

The p-type interconnect to the p+ DBR layer (AlGaInAs) was InSnO (ITO), which was rf sputter deposited to a thickness of 50nm. The ITO layer was deposited in a ratio of 5:1 of argon to oxygen at a total pressure of 5mTorr. A 200nm passivation of silicon dioxide was rf sputter deposited in order to dielectrically isolate the mesa structure and to provide some degree of additional sidewall protection. Sidewall coverage was achieved by rotating the wafer during sputter deposition. The contact to the n+ InP substrate was achieved through the sintered AuGeNi at 450C and 3 minutes. It is noted that the mesas were defined by reactive ion etching using a silicon nitride mesa etch mask which encapsulates the top metal contact.

3. 1. VCSEL SIMULATED PERFORMANCE AND EXPERIMENTAL EVALUATION

The simulation of the designed VCSEL performance has been carried out by evaluation of the important laser characteristics such as threshold gain, threshold current density and external quantum efficiency.

The material gain g_{th} required to reach threshold and to overcome the absorption losses in the investigated VCSEL was found to be equal to 198.32 cm^{-1} using the following equation (1) [18]:

$$N_w \Gamma_w \xi g_{th} = \alpha + \frac{1}{2L} ln \frac{1}{R_t R_b} \quad (1)$$

where N_w=8 is the number of quantum wells in the active region, Γ_w=0.015 [19] is the average optical confinement coefficient per quantum well, R_t=0.97 and R_b=0.999 are the reflectivities of the top and bottom Bragg mirrors, respectively, L=8949.9nm is the cavity length, and ξ=2 [20] is the energy confinement factor or gain enhancement factor where thin active layer is at the maxima of the electric field standing wave. The optical loss, α=30cm^{-1} [21], includes absorption in the cladding and active layers, and scattering due to defects and inhomogeneities in the lasing medium.

The threshold current density equal to J_{th} = 707.74 A/cm^2 with transparency current density of J_{tr} = 70.2 A/cm^2 [19] was calculated from the exponential dependence of J_{th}, on the device material parameters:

$$J_{th} = \frac{N_w J_{tr}}{\eta_i} exp\left(\frac{\alpha + \frac{1}{2L} ln \frac{1}{R_t R_b}}{N_w \Gamma_w \xi g_0} \right) \quad (2)$$

where η_I=0.9 [20] is the internal quantum efficiency, and g_0=1575cm^{-1} [22] is the material gain coefficient.

Assuming that VCSEL mesa structure has a diameter of 20μm, the threshold current would be I_{th} = 2.2 mA. The external quantum efficiency of the structure, η_d, equal to 0.33, is estimated using equation (3):

$$\eta_d = \eta_i \frac{ln \frac{1}{\sqrt{R_t R_b}}}{\alpha L + ln \frac{1}{\sqrt{R_t R_b}}} \quad (3)$$

Experimentally, the average threshold current measured for this design, with a 7μm device was 3mA. The comparison of the above parameters and calculations with other reported experimental results for the VCSELs lasing at 1.55μm showed that devices with strained MQW perform slightly better than the investigated laser, they have lower threshold current densities and transparency current densities [18,23], but the external quantum efficiencies are about the same as in this work. However, because of the optimization of the quaternary alloy parameters used in the VCSEL design, its characteristics are estimated to be better than other VCSELs with unstrained MQW active regions [19].

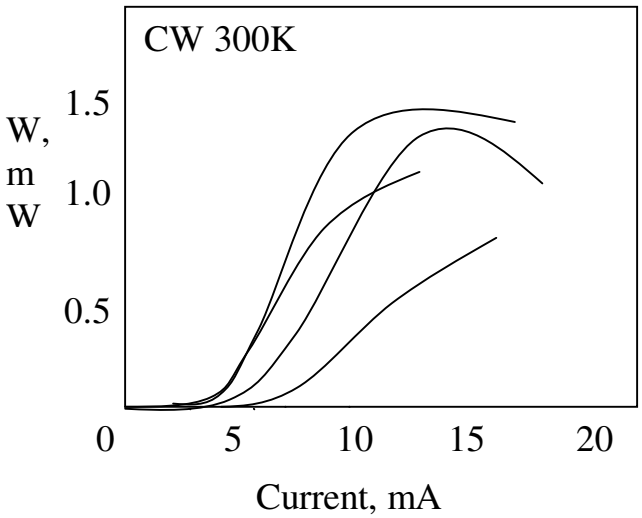

Figure 6. Light output, W [mW], vs current characteristics for oxidized 20μm devices

Figure 6 shows the light output versus current characteristics for laterally oxidized 20μm devices. Most of the devices which operated had threshold current less than 5mA and the average threshold current was 3mA. The threshold voltage was typically lower than 2.0V and the power output exceeded 1mW. The variation of threshold current is probably due to the variation in oxidation from mesa to mesa resulting in a variation of the recombination current component at the sidewall. The laser spectrum from a 7μm confined diode shows a single mode of operation at 1.54μm, very close to the designed value. The single fundamental mode was present at all current levels, and at the Bragg wavelength. The higher order modes have output powers reduced by at least 30-35 dB. The intermodal frequency separation was also considered and was found to be 1.5x10^{13} Hz. This intermode spacing indicates that only one mode will experience the high reflectivity and leads to a single mode oscillation. The oscillation spectrum measured again showed very strong suppression of the higher order modes. The peak wavelength of the spectrum was at 1542 nm with a peak amplitude of –3.5 dBm. These measurements indicate one specific advantage of VCSELs, that of attaining single mode operation without utilizing mode suppression or gain coupling measures.

4. SUMMARY

The present work demonstrates an effective design, fabrication method and performance of short (0.89μm) and long (1.546μm) wavelength VCSELs based on the optimization of the important material and laser parameters resulting in an overall reduction of the number of alternating layers used in DBRs as well as achieving a low threshold current values.

Acknowledgements

Funding by the Army Research Laboratory, the University of Maryland MRSEC, the NASA Space LIDAR Technology Center under the UMD-NASA cooperative agreement, and the COEDIP, are gratefully acknowledged.

References

[1] Miyamoto T, Uchida T, Yokouchi N, and Iga K, 1994 *J. Cryst. Growth*. **136** 210-215
[2] Tadokoro T, Okamoto H, Kohama Y, Kawakami T, and Kurokawa T, 1992 *IEEE Photon. Techn. Lett.* **4**(5) 409-411
[3] Choa F, Lee Y, Koch T, Burrus C, Tell B, Jewell J, and Leibenguth, *1991 IEEE Photon. Techn. Lett.* **3** 697-699
[4] Babic D, Streubel K, Mirin R, Margalit N, Bowers J, Hu E, Mars D, Yang L, and Carey K, 1995 *IEEE Photon. Techn. Lett*. **7**(11) 1225-1227
[5] Hansmann S, Walter H, Hillmer H, and Burkhard H, 1994 *J. Quant. Electron.* **30**(11) 2477-2483
[6] Rapp S, Piprek J, Streubel K, Andre J, and Wallin J, 1997 *J. Quant. Electron*. **33**(10) 1839-1845
[7] Delorme F, Grosmaire S, Gloukhian A, and Ougazzaden A, 1997 *Electron. Lett.* **33**(3) 210-211
[8] Debray J, Bouche N, Le Roux G, Raj R, and Quillec M, 1997 *Electron. Lett*. **33**(10) 868-869
[9] Blum O, Klem J, Lear K, Vawter G, and Kurtz S, 1997 *Electron. Lett.* **33**(22) 1878-1880
[10] Almuneau G, Genty F, Chusseau L, Bertru N, Fraisse B, and Jacquet J, 1997 *Electron. Lett*. **33**(14) 1227-1228
[11] Blum O, Fritz I, Dawtson L, and Drummond T, 1995 *Electron. Lett*. **31**(15) 1247-1248
[12] Harmand J, Kohl A, Juhel M, and Le Roux G, 1997 *J. Cryst. Growth* **175** 372-376
[13] Adachi S, 1987 *J. Appl. Phys*. **61**(10) 4869-4876
[14] Moon R, Antypas G, and James L, 1974 *J. Electr. Mater*. **3** (3) 635-644
[15] Adachi S, 1987 *Phys. Rev. B* **35**(14) 7454-7463
[16] Uomi K, Aoki M, Tsuchiya T, and Takai A, 1993 *IEEE J. Quant. Electron.* **29**(2) 355-360
[17] Weigl B, Grabherr M, Reiner G, and Ebeling K, 1996 *Electron. Lett.* **32**(6) 557-558
[18] Jones G, Smith A, O'Reilly E, Silver M, Briggs A, Fice M, Adams A, Greene P, Scarrott K, and Vranic A, 1998 *J. Quant. Electron***. 34**(5) 823-833
[19] Rosenzweig M, Mohrle M, Duser H, and Venghaus H, 1991 *J. Quant Electron*. **27**(6) 1805-1811
[20] Yang G, MacDougal M, Pudikov V, and Dapkus P, 1995 *IEEE Photon. Techn. Lett*. **7**(11), 1228-1230
[21] Iga K, Koyama F, and Kinoshita S, 1988 *J. Quant. Electron*. **24**(9) 1845-1855
[22] Makino T, 1996 *J. Quant. Electron.* **32**(3) 493-501
[23] Nichols D, Sherwin M, Munns G, Pamulapati J, Loehr J, Singh J, Bhattacharya P, and Ludowise M, 1992 *IEEE J. Quant. Electron.* **28**(5) 1239-1242